Pergamon

Int. J. Heat Mass Transfer. Vol. 39, No. 8, pp. 1697–1710, 1996

0017-9310/96 $15.00+0.00

0017-9310(95)00251-0

Numerical simulation of transitional aiding mixed convective air flow in a bottom heated inclined rectangular duct

C. C. HUANG† and T. F. LIN‡

Department of Mechanical Engineering, National Chiao Tung University, Hsinchu, Taiwan, Republic of China

(*Received* 18 *July* 1994 *and in final form* 27 *June* 1995)

Abstract—Buoyancy induced transient transitional flow structures and the associated heat transfer in mixed convective aiding flow of air in a bottom heated inclined rectangular duct were numerically investigated. The three-dimensional unsteady Navier–Stokes and energy equations were discretized by higher order finite-difference approximations and directly solved by the projection method. Computations were carried out for the Reynolds number ranging from 100 to 500, aspect ratio of the duct from 2 to 4, duct inclination from 0° to 60°C and buoyancy-to-inertia ratio high enough to cause flow transition. Attention was particularly paid to delineate the effects of the duct inclination on the flow transition and the associated temporal and spatial flow structures. It is of interest to note from the predictions that increasing the inclined angle measured from horizontal does not always stabilize the flow. In fact, the flow stability is highly dependent on all the governing parameters and is intimately related to the structural changes in the buoyancy induced longitudinal vortices.

1. INTRODUCTION

A simple forced convective duct flow and heat transfer in it can be significantly modified when subject to high buoyancy force. The understanding of this modification of flow and thermal structures in a rectangular duct is important in various technological processes, such as cooling of microelectronic equipments, growing of single crystal from chemical vapor deposition and energy transfer in compact heat exchangers. In a mixed convective flow through a bottom heated horizontal rectangular duct, the buoyancy force is normal to the forced flow direction and usually steady longitudinal vortex rolls are induced as Gr/Re^2 exceeds a certain critical value. At a higher Gr/Re^2, the flow may become unstable and transitional. The buoyancy force, however, is no longer normal to the forced flow in an inclined duct. In fact, it can be decomposed into two components: one normal to and another parallel with the forced flow. Again, the normal component tends to induce longitudinal rolls, but the parallel component can accelerate or decelerate the flow, depending on their relative orientation to the forced flow. For aiding buoyancy the flow acceleration in the near-bottom region and deceleration in the near-top region by the parallel buoyancy component is expected to distort the vortices generated by the normal component and the flow can become less stable. On the other hand, the normal component is smaller for a larger inclination measured from horizontal, and hence, fewer vortices are generated and they are weaker. This produces a stabilizing effect. But when the vortices are too weak, they tend to disintegrate, which may destabilize the flow. Therefore, two opposite effects are present at the same time for an increase in duct inclination. Whether the resulting flow is stabilized or destabilized by the duct inclination depends on the particular set of parameters investigated. This study intends to investigate the complex transitional vortex flow in an inclined rectangular duct under buoyancy aiding condition, through a three-dimensional time-accurate numerical simulation. Effects of the governing parameters—the inclined angle ϕ, aspect ratio of the duct A and Reynolds and Grashof numbers, Re and Gr, on the flow and thermal characteristics will be examined in detail.

A considerable amount of work has been carried out in the literature to study the mixed convective flow in a horizontal plane channel. A detailed review of the early work was already given by our earlier study [1]. These previous studies are briefly reviewed here. The onset of thermal instability was experimentally and theoretically predicted [2–5]. Characteristics of the steady and unsteady vortex rolls were experimentally observed by Ostrach and Kamotani [2] and by Chiu and Rosenberger [6] and Chiu *et al.* [7]. More experimental data for the vortex flow and convective heat transfer coefficient were provided in refs. [8, 9]. Numerical simulation of the steady longitudinal vortex rolls was conducted by a number of studies [4, 10–

† Dr C. C. Huang presently works at Center for Industrial Safety and Health Technology, Industrial Technology Research Institute, Hsinchu, Taiwan, Republic of China.

‡ Author to whom correspondence should be addressed.

NOMENCLATURE

A aspect ratio, b/d
b, d width and height of the duct
g gravitational acceleration
Gr modified Grashof number, $g\beta q''_w d^4/kv$
h local convection heat transfer coefficient
k thermal conductivity
ℓ, L dimensional and dimensionless length of the heated plate
Nu Nusselt number, hd/k
P, p_m dimensionless and dimensional dynamic pressures, $p_m/\rho\bar{w}_e^2$
Pr Prandtl number, v/α
q''_w wall heat flux
Re Reynolds number, $\bar{w}_e d/v$
t, τ dimensional and dimensionless time, $t/(d/\bar{w}_e)$
T, θ dimensional and dimensionless temperatures, $(T-T_e)/(q''_w d/k)$
u, v, w velocity components in x, y, z directions
U, V, W dimensionless velocity components in X, Y, Z directions, $u/\bar{w}_e, v/\bar{w}_e, w/\bar{w}_e$
x, y, z Cartesian coordinates
X, Y, Z dimensionless Cartesian coordinates, $x/d, y/d$ and z/d
Z^+ modified Z coordinate, $Z/(Re\ Pr)$.

Greek symbols
α thermal diffusivity
β thermal expansion coefficient
v kinematic viscosity.

Subscripts
e values at the duct inlet
fd fully developed
p period
w of wall qualities.

Superscripts
$\bar{}$ average value.

12]. Extensive studies were also performed in the past to investigate mixed convection in a vertical plane channel. A simple numerical analysis of the unidirectional flow at low buoyancy was given by Aung and Worku [13], Chow *et al.* [14] and Yao [15]. The buoyancy induced recirculating flow was experimentally visualized [16, 17] and numerically predicted [18, 19] in several studies. Effects of the channel inclination on the vortex flow have not received enough attention. Fukui *et al.* [20] experimentally and numerically investigated a steady fully developed mixed convective plane channel flow with $Ra(=Gr\times Pr) < 9300$ and $\phi \leqslant 32.1°$. In the horizontal flow the interaction between vortices was found to be rather small. However, in the inclined flow the neighboring vortices tend to form a pair with a single velocity peak. Numerical computation from Naito and Nagano [21] investigated the buoyancy effects in the entrance region covering a wide range of inclination angle, but at subcritical Rayleigh numbers. Thus no vortex flow is formed and steady two-dimensional simulation is suitable. The critical condition for the appearance of the flow reversal was proposed. Experimental data for the local and average Nusselt number were provided by Morcos *et al.* [22] and Maughan and Incropera [9]. The above literature review clearly indicates that the detailed characteristics of the buoyancy induced flow transition from steady laminar to unsteady but periodic laminar state and finally to unsteady irregular, turbulent state are still poorly understood, especially for an inclined duct. In an initial attempt to explore the vortex flow transition, the present authors recently conducted a three-dimensional unsteady direct numerical simulation of the mixed air convective flow in a horizontal duct of aspect ratio fixed at 2 and Reynolds number at 500 [1]. At increasing buoyancy, the flow transition was found to follow the Rulle–Taken route [23]. An extension is made here to investigate the mixed convective flow transition in an inclined rectangular duct.

Figure 1 shows the schematic of the physical model to be investigated along with the coordinate system chosen. Initially at time $t < 0$, the air flow is fully developed and the isothermal at T_e in a thermally well insulated inclined rectangular duct of width b and

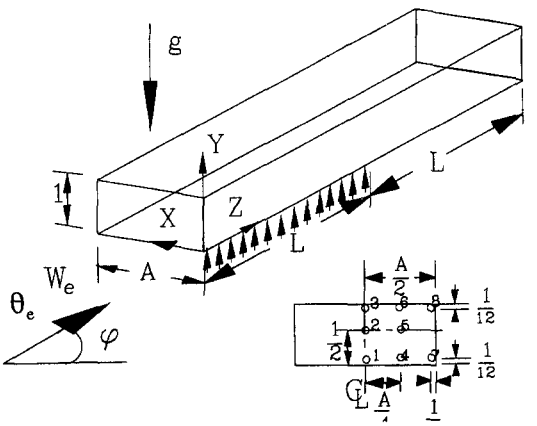

Fig. 1. Schematic of the physical system and the selected detection points at a cross section (the X and Y coordinates at various points are as follows: point 1—($A/2$, 1/12), 2—($A/2$, 1/2), 3—($A/2$, 11/12), 4—($A/4$, 1/12), 5—($A/4$, 1/2), 6—($A/4$, 11/12), 7—(1/5, 1/12), 8—(1/5, 11/12)).

height d. At $t = 0$, a uniform heat flux q''_w is suddenly imposed at the bottom plate over a finite length ℓ and maintained at this level thereafter. The initially unidirectional steady flow is significantly modified as the heating level is high enough, so that the first critical Rayleigh number Ra (the onset of vortex flow) and second critical Rayleigh number (the appearance of time periodic flow) are exceeded. The evolution of these complicated flows will be carefully examined.

2. MATHEMATICAL MODELLING

When the length, time, velocity and temperature are, respectively, scaled with the duct height d, residence time of the flow $d/\bar{w}_e$, average velocity of the forced flow $\bar{w}_e$ and conductive temperature unit $q''_w d/k$, the basic equations describing the temporal and spatial evolution of the buoyancy induced vortex flow of a Boussinesq fluid through an inclined duct studied here, are

$$\frac{\partial U}{\partial X}+\frac{\partial V}{\partial Y}+\frac{\partial W}{\partial Z}=0 \tag{1}$$

$$\frac{\partial U}{\partial \tau}+U\frac{\partial U}{\partial X}+V\frac{\partial U}{\partial Y}+W\frac{\partial U}{\partial Z}=-\frac{\partial P}{\partial X}+\frac{1}{Re}\left(\frac{\partial^2 U}{\partial X^2}+\frac{\partial^2 U}{\partial Y^2}+\frac{\partial^2 U}{\partial Z^2}\right) \tag{2}$$

$$\frac{\partial V}{\partial \tau}+U\frac{\partial V}{\partial X}+V\frac{\partial V}{\partial Y}+W\frac{\partial V}{\partial Z}=-\frac{\partial P}{\partial Y}+\frac{1}{Re}\left(\frac{\partial^2 V}{\partial X^2}+\frac{\partial^2 V}{\partial Y^2}+\frac{\partial^2 V}{\partial Z^2}\right)+\frac{Gr}{Re^2}\theta\cos\phi \tag{3}$$

$$\frac{\partial W}{\partial \tau}+U\frac{\partial W}{\partial X}+V\frac{\partial W}{\partial Y}+W\frac{\partial W}{\partial Z}=-\frac{\partial P}{\partial Z}+\frac{1}{Re}\left(\frac{\partial^2 W}{\partial X^2}+\frac{\partial^2 W}{\partial Y^2}+\frac{\partial^2 W}{\partial Z^2}\right)+\frac{Gr}{Re^2}\theta\sin\phi \tag{4}$$

$$\frac{\partial \theta}{\partial \tau}+U\frac{\partial \theta}{\partial X}+V\frac{\partial \theta}{\partial Y}+W\frac{\partial \theta}{\partial Z}=\frac{1}{RePr}\left(\frac{\partial^2 \theta}{\partial X^2}+\frac{\partial^2 \theta}{\partial Y^2}+\frac{\partial^2 \theta}{\partial Z^2}\right). \tag{5}$$

Three governing physical parameters in the above formulation are the buoyancy-to-inertia ratio Gr/Re^2, Reynolds number Re and Prandtl number Pr. They are defined as

$$\frac{Gr}{Re^2}=\frac{g\beta q''_w d^2}{k\bar{w}_e^2} \quad Re=\frac{\bar{w}_e d}{\nu} \quad Pr=\frac{\nu}{\alpha}. \tag{6}$$

The problem is subject to the following initial and boundary conditions:

$\tau = 0$;

$$U = V = \theta = W - W_{fd} = 0$$

$\tau \geqslant 0$;

at $Z = 0$ $\quad U = V = \theta = W - W_{fd} = 0$

at $Z \to \infty$ $\quad \dfrac{\partial U}{\partial Z}=\dfrac{\partial V}{\partial Z}=\dfrac{\partial \theta}{\partial Z}=\dfrac{\partial W}{\partial Z}=0$

at $Y = 0$ and $Z \leqslant L$

$$\frac{\partial \theta}{\partial Y}+1 = U = V = W = 0$$

at all other surfaces, $\dfrac{\partial \theta}{\partial n} = U = V = W = 0$, (7)

where n is a unit normal to a surface and W_{fd} is the fully developed velocity. Based on a vast amount of experimental data, W_{fd} is correlated by Holes and Vermmeulen [24] as

$$W = W_{fd} = \left(\frac{m+1}{m}\right)\left(\frac{n+1}{n}\right) \times [1-(|2Y-1|)^n]\left[1-\left(\left|\frac{2X}{A}-1\right|\right)^m\right], \tag{8}$$

where values of the constants m and n depend on the aspect ratio.

The local Nusselt number signifies the heat transfer from the bottom heated plate to the channel flow and is based on the difference in the bottom temperature T_w and inlet temperature T_e. It is defined and evaluated as

$$Nu=\frac{hd}{k}=\frac{q''_w}{(T_w-T_e)}\frac{d}{k}=\frac{1}{\theta_w}\bigg|_{y=0}. \tag{9}$$

3. NUMERICAL SOLUTION

In view of the nonlinearity in the inertia terms, the basic equations were solved numerically. In particular, the projection method (Peyret and Taylor [25]) was chosen here to integrate the equations on a staggered grid system. To enhance the numerical accuracy and stability, all the spatial derivatives were discretized by the fourth-order central difference (Hirsch [26]) except the convective terms which were approximated by the third-order upwind difference proposed by Kawamura *et al.* [27]. To allow for the possible asymmetric flow with respect to the central vertical plate at $X = A/2$ for the time dependent flow at high buoyancy, the computation domain in the spanwise direction includes both the left half ($0 \leqslant X \leqslant A/2$) and right half ($A/2 \leqslant X \leqslant A$) of the duct. Although the downstream boundary conditions were exactly specified at $Z \to \infty$, only a finite unheated section is added in the downstream to facilitate the numerical analysis. This added unheated section must be long enough so that the solution for the problem is independent of its

size. Numerical tests indicated that the suitable length for the down-stream unheated section is $L/3$. To ensure the results are independent of the added section length, it is chosen to be L in the computation.

The first-order Euler explicit scheme was employed here to treat the time derivatives. We also found that the first-order scheme was sufficiently accurate to resolve the smallest physical time scale. The stability of the scheme is limited by requirement that the Courant number be less than unity (Anderson *et al.* [28]). To ensure the numerical convergence, the Courant number is set below 0.2 in the computation, which leads to

$$\Delta\tau < 0.2 \times \text{minimum}\left(\frac{\Delta X}{U_{\max}}, \frac{\Delta Y}{V_{\max}}, \frac{\Delta Z}{W_{\max}}\right). \quad (10)$$

The sequence of numerical operation is as follows:

(1) Explicitly calculate the provisional velocity.

(2) Solve the pressure equation by the vectorized Gauss–Seidel method with successive overrelaxation. The solution for the pressure is considered as convergent when the mean relative pressure difference between two consecutive iterations is below 10^{-4}. A similar criterion is employed to ensure that the mass residual is less than 10^{-4} at each node, at each time step.

(3) Explicitly calculate the desired velocity and temperature fields at the new time step. Procedures 1–3 were repeatedly applied from the initiation of the transient to a final steady state or to a statistical state when the flow was no longer steady for a long time. The flow is considered at statistical state when its time-average quantities do not vary with time.

For a low Reynolds number flow considered ($Re \leqslant 500$), a uniform grid is placed in the computational domain with the number of nodes in the X, Y, Z-directions—I, J and K varied from 31 to 61, depending on the particular set of parameters to be investigated.

To verify the proposal numerical scheme, a series of stringent program tests were conducted. First, the predicted spanwise average Nusselt number variations with the axial coordinate for the pure forced convection ($Gr/Re^2 = 0$) of air in a rectangular duct were found to be in excellent agreement with the numerical and experimental results of Maughan and Incropera [9]. Then, the steady mixed convection of nitrogen in a high aspect ratio horizontal rectangular duct was simulated. The comparison of the computed axial velocity profiles for a typical case with $Pr = 0.7$, $Re = 44.8$, $Gr/Re^2 = 3.43$ and $A = 10$ with the experimental data of Chiu *et al.* [7] shows good agreement [1]. Further comparison was made to test the data of Ostrach and Kamotani [2] for the spanwise temperature distributions. The agreement is also good. Finally, a grid test was performed. Sampled results from such a test are compared in Fig. 2 for the spanwise average Nusselt number at $\tau = 240$ and time variations of θ and W at two selected locations for τ between 180–220 for a typical case with $Pr = 0.7$, $Re = 100$, $Gr/Re^2 = 90$, $A = 4$ and $\phi = 60°$. Note that the difference in the results from using the grids $51 \times 41 \times 41$ and $61 \times 51 \times 51$ is less than 3%. Thus I, J and K were, respectively, chosen to be larger than 51, 41 and 41 in the subsequent calculation. Through these program tests, the adopted solution procedures are considered to be suitable for the present study.

4. RESULTS AND DISCUSSION

The above problem formulation clearly indicates that the flow to be investigated is governed by the Prandtl and Reynolds numbers, the buoyancy-to-inertia ratio Gr/Re^2, the inclination angle ϕ, aspect ratio of the duct A and the nondimensional length of the bottom heated plate $L(=\ell/d)$. Systematic computation was carried out for air flow ($Pr = 0.72$) in a rectangular duct of aspect ratio $A = 2$ and 4, inclined from horizontal by 0°–60° with the Reynolds number varying from 100 to 500 and L fixed at 20. The buoyancy-to-inertia ratio is varied from low to high values so that flow transition occurs. In the present three-dimensional unsteady flow calculation, a vast amount of numerical data were obtained. Only a very small sample of these results are to be presented here, to mainly delineate the effects of various parameters on the characteristics of mixed convective flow transition in an inclined duct. Complete results are available from our report [29]. It is noted in the computation that the predicted velocity and temperature fields are symmetric with respect to the vertical central plane at $X = A/2$, except for a highly chaotic flow in which a slight flow asymmetry appears. Thus, only the results in the left or right half of the duct will be given. Attention is focused on the flow characteristics at a steady or statistical state when the initial transient has elapsed.

4.1. *Effects of the duct inclination*

To illustrate the effects of the duct inclination on the flow transition, results for various inclined angles are presented for $Re = 500$, $Gr/Re^2 = 30$ and $A = 2$. For comparison purpose, the results for the time histories of the axial velocity W at selected detection points specified in Fig. 1, at three selected cross sections along with the temperature contours and cross plane streamlines at various cross sections in a typical period obtained in the previous study [1] for a horizontal duct ($\phi = 0°$), are shown in Fig. 3. Note that the buoyancy induced secondary flow is in the form of two pairs of longitudinal vortex rolls (Fig. 3a). The vortex flow intensity is nonmonotonic in the axial direction and changes significantly with time, as evident from the values of the streamfunctions. Also the roll size varies substantially with space and time. The time histories in Fig. 3b for W and the time records

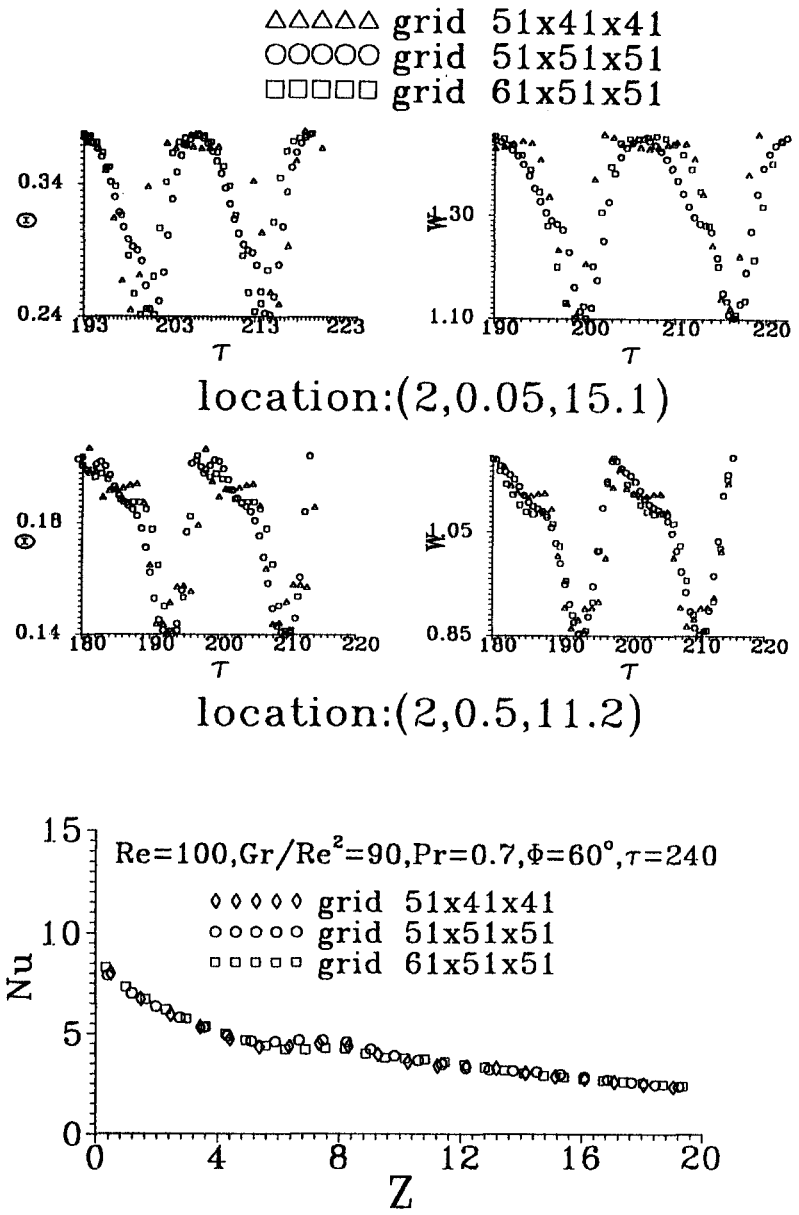

Fig. 2. Time histories of W and θ at two locations and axial variations of the spanwise average Nusselt number at $\tau = 240$ calculated from various grids for $Pr = 0.7$, $Re = 100$, $Gr/Re^2 = 90$, $A = 4$ and $\phi = 60°$.

for θ, which are not shown here for the reason of limited space available for the article, indicate that in the entry portion of the heated section the flow oscillation is mainly characterized by a single fundamental frequency f_1 ($=0.266$) and its harmonics. Thus the flow is time periodic. A close inspection of the power spectrum densities for the time histories, however, discloses that at locations 4 and 5 a second fundamental mode f_2 ($=0.320$) already appears, implying that the flow around these locations is quasiperiodic. Downstream of the entry portion the flow is mainly quasiperiodic. Near the exit end of the heated section ($Z \geqslant 12$) the flow is chaotic.

Results for $\phi = 30°$ are examined next. Figure 4 presents the secondary vortex flow patterns and isotherms in a typical period and the time records of the axial velocity for an inclination angle of 30° with other parameters fixed at the same values as those in Fig. 3. These results when contrasted with those in Fig. 3 for $\phi = 0°$ suggest that at $\phi = 30°$ the flow oscillates periodically at a much lower single fundamental frequency $f_1 = 0.09$ in the entire duct. But the oscillation amplitude is higher in a number of detected locations for the inclined case. Besides, the intensity of the secondary flow is weaker at $\phi = 30°$ by comparing the streamfunction values. Furthermore, there are also two pairs of vortices in the duct at $\phi = 30°$. But the vortices in the duct core are bigger and stronger than

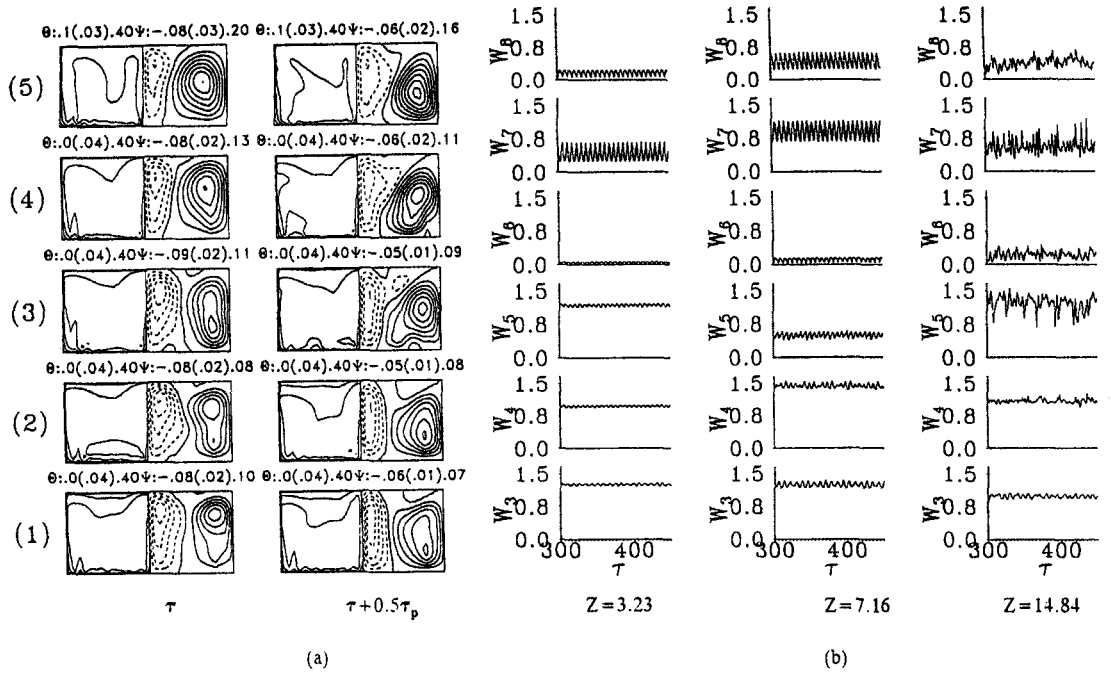

Fig. 3. (a) Isotherms and cross plane streamlines at cross sections (1)$Z = 2.93$, (2)$Z = 4.88$, (3)$Z = 6.83$, (4)$Z = 8.78$, (5)$Z = 10.73$ in a typical period, the period of the flow τ_p is 3.76; and (b) time histories of W at selected detection points at three cross sections (W_i denotes W at detection point i) for $Re = 500$, $Gr/Re^2 = 30$, $\phi = 0°$ and $A = 2$.

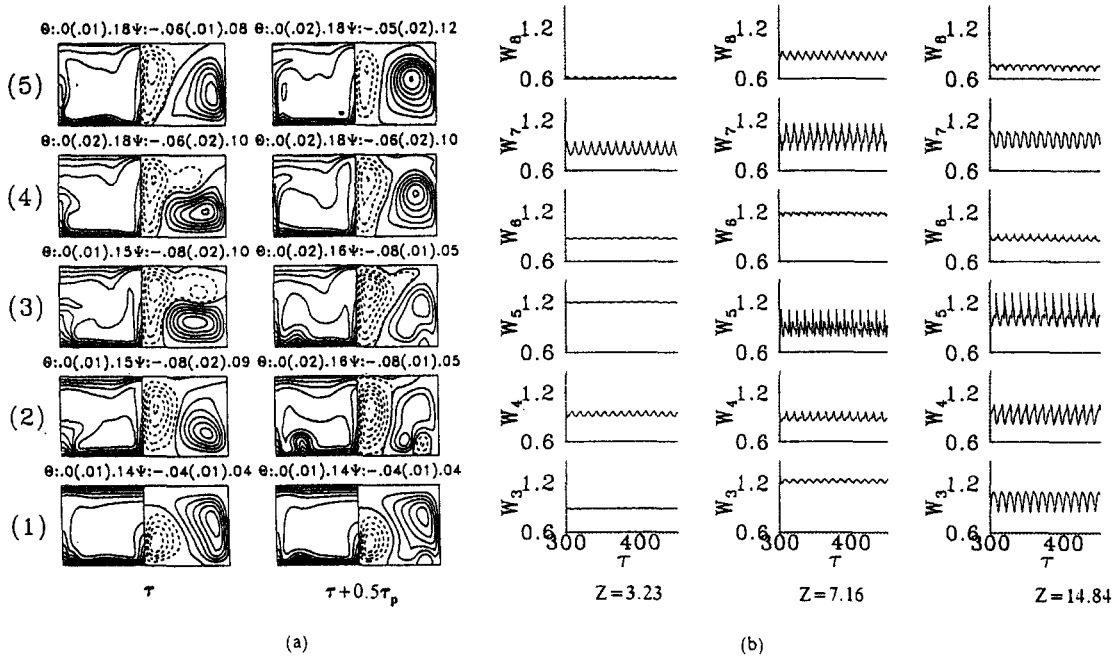

Fig. 4. (a) Isotherms and cross plane streamlines at cross sections (1)$Z = 2.93$, (2)$Z = 4.88$, (3)$Z = 6.83$, (4)$Z = 8.78$, (5)$Z = 10.73$ in a typical period ($\tau_p = 11.41$) and (b) time histories of W at selected detection points at three cross sections for $Re = 500$, $Gr/Re^2 = 30$, $\phi = 30°$ and $A = 2$.

those near the side walls. In summary, inclining the duct from 0 to 30° causes the flow to change from a transitional quasiperiodic and chaotic state to a periodic (more regular) state with a larger oscillation amplitude, but smaller secondary flow intensity. Thus a stabilizing effect is produced for inclining the duct from 0 to 30°.

As the duct is further inclined to 45°, the flow becomes chaotic in the entire duct, as evident from the time histories given in Fig. 5. Now a destabilizing effect on the flow is produced for the duct inclining from 30 to 45°. In addition, the results suggest that the flow fluctuates very slowly in time, but in very large amplitude. The cause of the flow to become chaotic can be attributed to the significant change in the flow pattern for $\phi = 45°$. Note that at $\phi = 45°$ the normal buoyancy component is smaller and only a pair of vortices are induced in the entry region. Slightly downstream, another pair of vortices are induced, sometimes near the lower corners and at other times near the central portion of the heated plate. Further downstream, only those in the duct core grow and they gradually become stronger than the original vortices, and may squeeze the original pair near the side walls in the exit region. Some additional small cells are also induced near the heated plate in this region. As a result, the longitudinal vortex rolls are highly distorted and the flow is unstable. Comparing the streamfunction values in Fig. 5 with those in Fig. 4 manifests that the secondary flow is weaker for $\phi = 45°$ only in the entry region. Downstream the secondary flow is stronger.

At an even higher inclined angle of 60°, the flow is found to be steady in the first half of the duct ($Z \leqslant 10$) and time periodic in the second half. The periodic flow evolution shows that only a pair of longitudinal vortex rolls are induced except in the exit region. The flow oscillation in the second half of the duct is at a lower frequency of $f_1 = 0.062$. The oscillation amplitude is, however, not small. Thus inclining the duct from 45 to 60° results in a stabilizing effect on the flow.

Finally, the effects of the duct inclination on the distributions of the heated plate temperature and local Nusselt number are presented in Fig. 6. Note that in the region where the cross plane vortex flow is stronger the local Nusselt number is higher and the plate temperature is lower.

4.2. *Effects of the aspect ratio*

Results from another series of computations for a wider duct of $A = 4$, $Re = 100$, $Gr/Re^2 = 90$ and $\phi = 0°$, 30° and 60° are presented here to illustrate the effects of the aspect ratio on the mixed convective flow transition in an inclined duct. The predicted results for the base case shown in Fig. 7 is the flow in a horizontal duct ($\phi = 0°$). The time histories for W suggest that the flow in the entire duct is time periodic and is characterized by a single fundamental mode at $f_1 = 0.093$ and its harmonics. It is important to note that the amplitudes of the θ and W oscillations are larger in the lower half of the duct, except in the exit region and do not always increase with the downstream distance. More precisely, the flow near the top unheated plate is nearly steady. Inspecting the time evolution of the secondary vortex flow in a period reveals that over a certain part of the period the rolls near the side walls disintegrate at $Z = 3.87$, resulting in four pairs of longitudinal rolls in the duct. The disintegration is conjectured to be caused by the additional thermals driven by the unstable thermal boundary layer on the heated bottom plate. These thermals are rather weak and the rolls are found to merge later near the duct exit. It is further noted that the rolls are smaller in the vertical extent, as compared with those in Fig. 3 for $A = 2$, and only occupy the bottom half of the duct. A stable thermal stratification is resulted in the top half of the duct. This, in turn, damps the flow oscillations out and stabilizes the flow in this region, as reflected in the time histories just discussed.

As the duct is tilted by 30°, the flow is found to be steady at long time. It is important to note from the steady flow patterns shown in Fig. 8a that the two pairs of longitudinal rolls for $\phi = 30°$ are much larger than those for the horizontal duct and nearly occupy the entire duct. Thus, no stable thermal stratification occurs in the upper half of the duct, as supported by the isotherms. As the duct is further tilted to 60°, the flow becomes time periodic again after the initial transient. Thus, there exists a reverse flow transition for raising the inclined angle for $A = 4$. The results indicate that at $\phi = 60°$, over a certain time interval, the rolls disintegrate from two pairs to three pairs in the upstream region near the inlet and later in the downstream region near the exit of the heated section they recombine into two pairs. Inspecting the flow patterns closely for various ϕ suggests that the secondary vortex flow is stronger when the duct is inclined from 0 to 30°. But the opposite trend is noted for further inclining the duct from 30 to 60°.

4.3. *Effects of the Reynolds number*

To explore the influences of the Reynolds number on the flow transition in an inclined duct, results for $Re = 200$ and 400 are examined in the following for various inclined angles. The predicted time samples of W at location 5 at various cross sections for $Re = 200$ are presented in Fig. 9 for various inclined angles with $Gr/Re^2 = 62.5$ and $A = 4$. These results indicate that at $\phi = 0°$ the flow is periodic in the first half of the duct and becomes quasiperiodic downstream of this region. Nonperiodic flow prevails in the entire duct at $\phi = 30°$. At $\phi = 45°$ large amplitude chaotic flow is prevalent, except in the duct entry. Flow returns to a time periodic state for $\phi = 60°$ in the entire duct. The corresponding instantaneous flow patterns are given in Fig. 10 at selected time instants. The results for $\phi = 0°$, when contrasted with those in Fig. 7 for $Re = 100$ and $\phi = 0°$, indicate that at $Re = 200$ the induced vortex rolls are somewhat larger, so that the

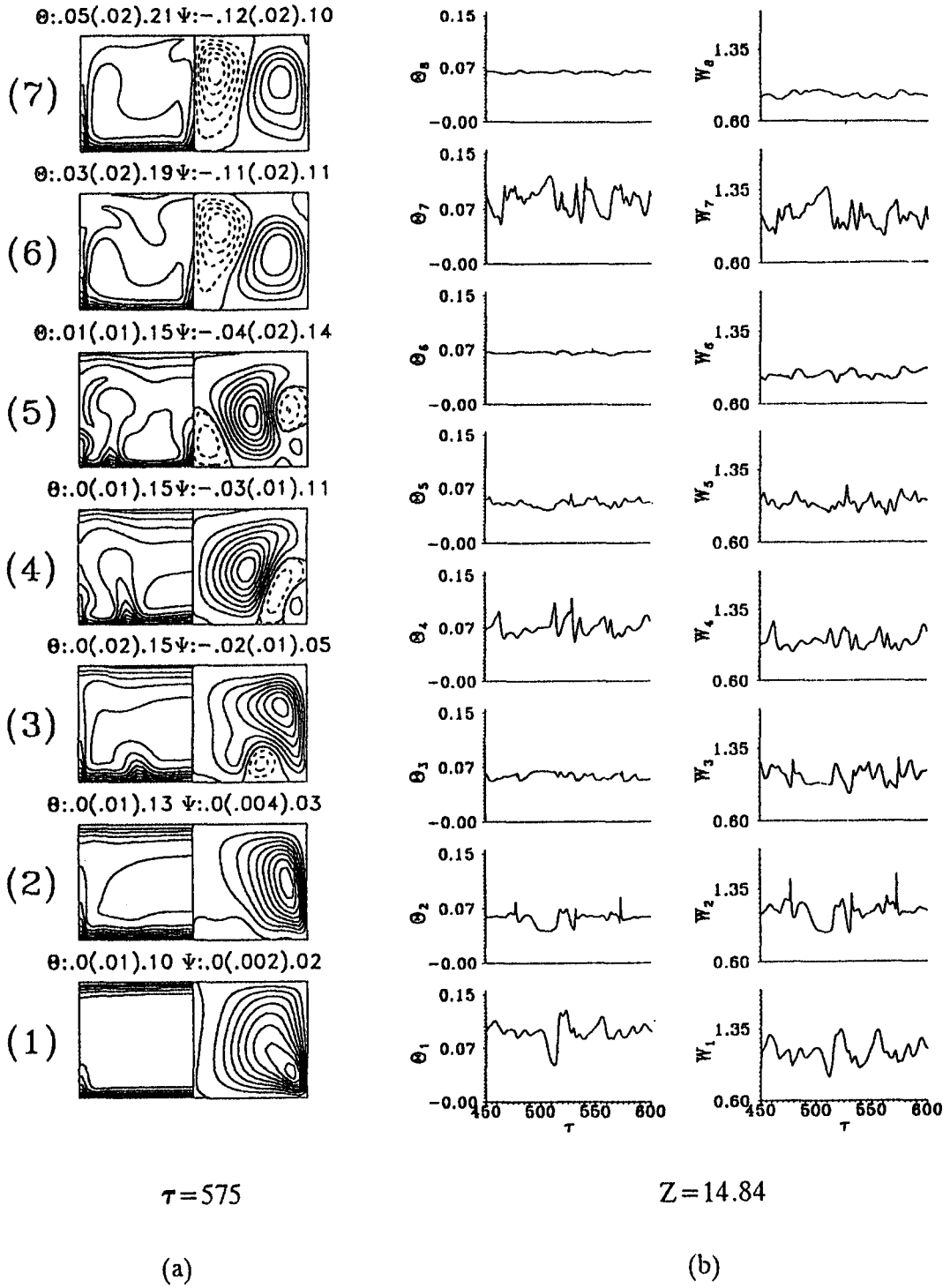

Fig. 5. (a) Isotherms and cross plane streamlines at cross sections (1)$Z = 0.98$, (2)$Z = 2.93$, (3)$Z = 4.88$, (4)$Z = 6.83$, (5)$Z = 8.78$, (6)$Z = 12.63$ and (7)$Z = 16.49$ for $\tau = 575$ and (b) time samples of θ and W at selected detection points at cross section $Z = 14.87$ for $Re = 500$, $Gr/Re^2 = 30$, $\phi = 45°$ and $A = 2$.

stable thermal stratification is confined in a smaller region near the top plate. Besides, for $\phi = 0°$ the structure of the longitudinal rolls remains nearly the same for the entire duct ($Z \leqslant 15$), except near the duct exit where the cell breakup occurs. In this cell breakup region the flow is rather unstable. It is noted from the complete numerical data that the flow oscillates time periodically in a small amplitude, except in the exit region where the oscillation quickly intensifies and becomes highly irregular, obviously due to the cell

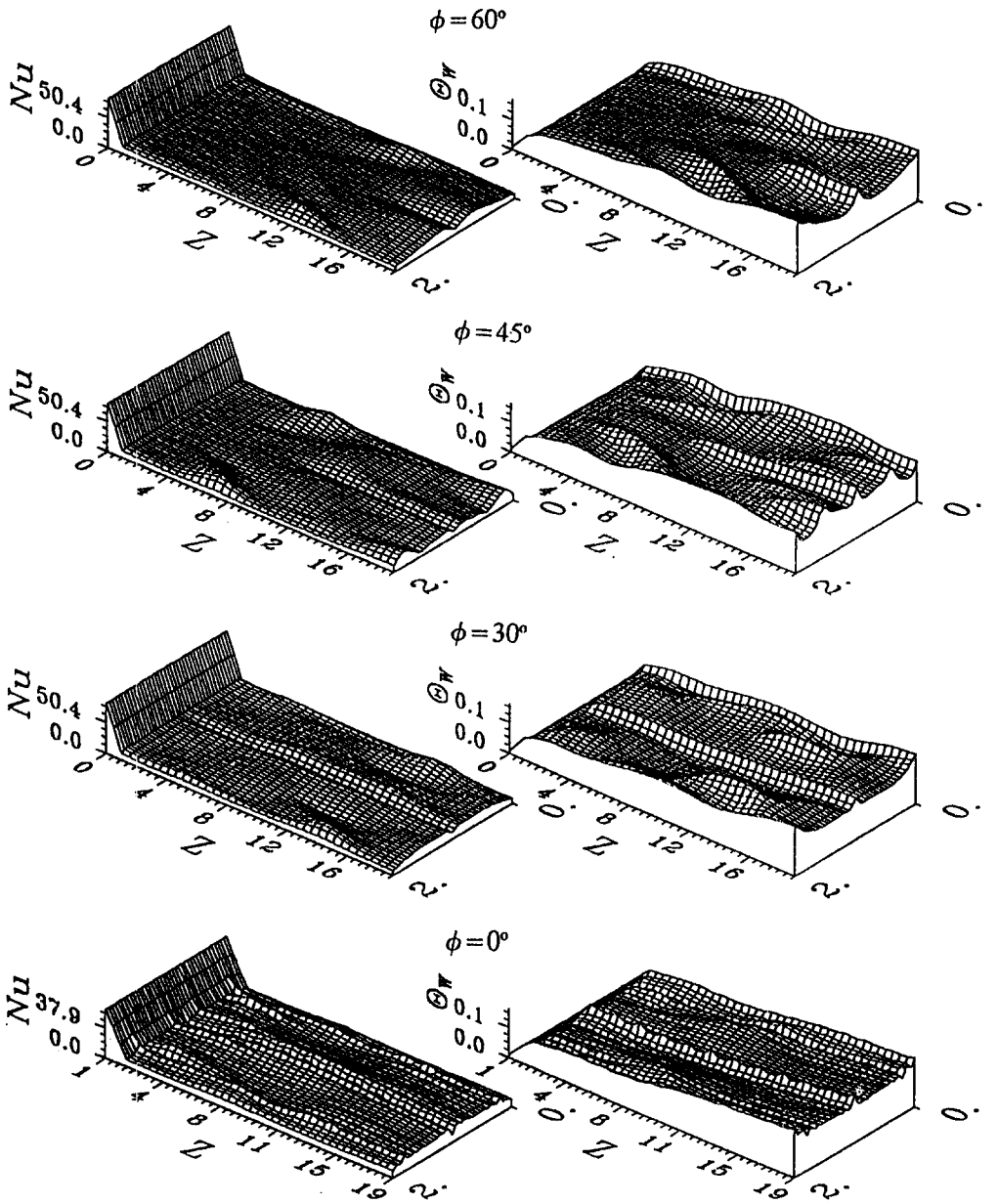

Fig. 6. The local Nusselt number and temperature distributions on the heated bottom plate for various inclined angles for $Re = 500$, $Gr/Re^2 = 30$ and $A = 2$ at large τ.

disintegration. Moreover, the flow at $Re = 200$ oscillates at a much higher frequency ($f_1 = 0.267$), as compared with that for $Re = 100$ ($f_1 = 0.077$).

For a duct tilted by 30° at $Re = 200$ the cells disintegrate and merge in the entry half of the duct and the processes repeat irregularly. Besides, the secondary flow intensity varies significantly with the axial distance in this region and is much stronger than that for $\phi = 0°$. In the downstream the roll structure does not experience drastic change. The time samples shown in Fig. 9 for $\phi = 30°$ do concur with the above observation. It is also observed that the chaotic flow oscillates at much higher frequencies in regions near the side walls (locations 7 and 8) than those in other regions. The decay in the oscillation amplitude with the axial distance is clearly seen, mainly in the immediate downstream of the duct entry. It is also worth mentioning that at $\phi = 30°$ the rolls are bigger than those at $\phi = 0°$.

For a larger inclined angle of 45° the flow is highly irregular. The breakup and merge of the vortices are more frequent in both time and space. Significant variations in the vortex flow intensity are observed. The vortex flow intensity is slightly weaker than that for $\phi = 30°$. The oscillation amplitude increases sharply with the axial distance in the entry region and decays gradually in the downstream. To enhance our understanding of the three-dimensional vortex flow

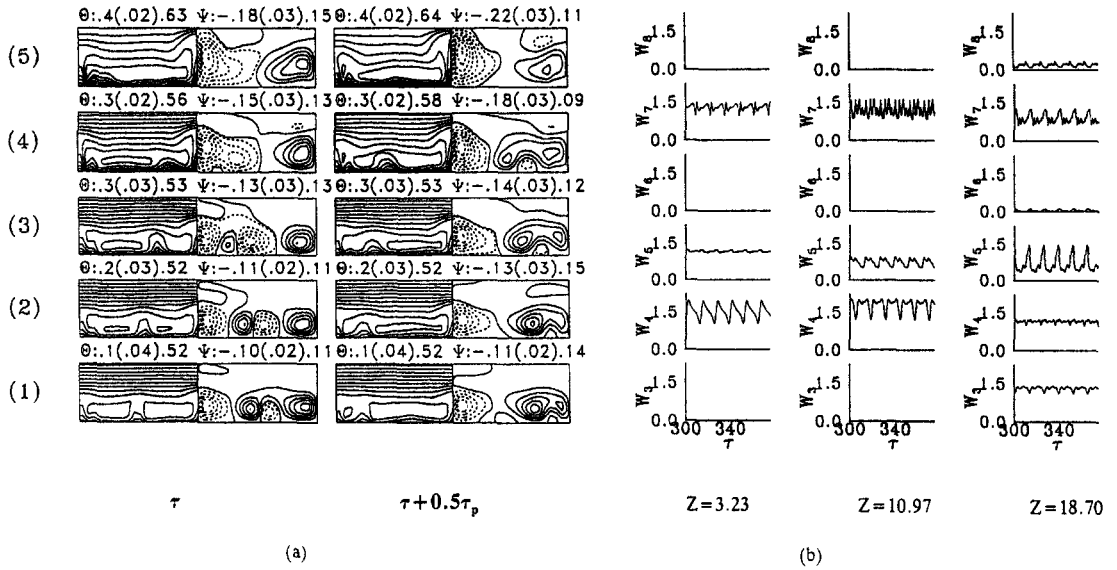

Fig. 7. (a) Isotherms and secondary flow in a typical period ($\tau_p = 12.99$) at cross sections (1)$Z = 3.87$, (2)$Z = 6.45$, (3)$Z = 9.02$, (4)$Z = 11.61$, and (5)$Z = 14.19$ and (b) time records of W at selected detection points at various cross sections for $Re = 100$, $Gr/Re^2 = 90$, $\phi = 0°$ and $A = 4$.

structure, the predicted flow is also viewed from the side and top. The results show the flow acceleration near the heated bottom plate in the entry region. This accelerated flow is later deflected away or toward the bottom plate, depending on the spanwise location, by the longitudinal vortices driven by the normal buoyancy component as it proceeds downstream. The top view of the flow clearly manifests the roll breakup and merge mentioned above.

Inspecting the periodic flow evolution for $\phi = 60°$ and the associated time records for θ and W reveals that the structure of the longitudinal rolls changes substantially shortly after the flow enters the heated section and proceeds for some distance, and the flow

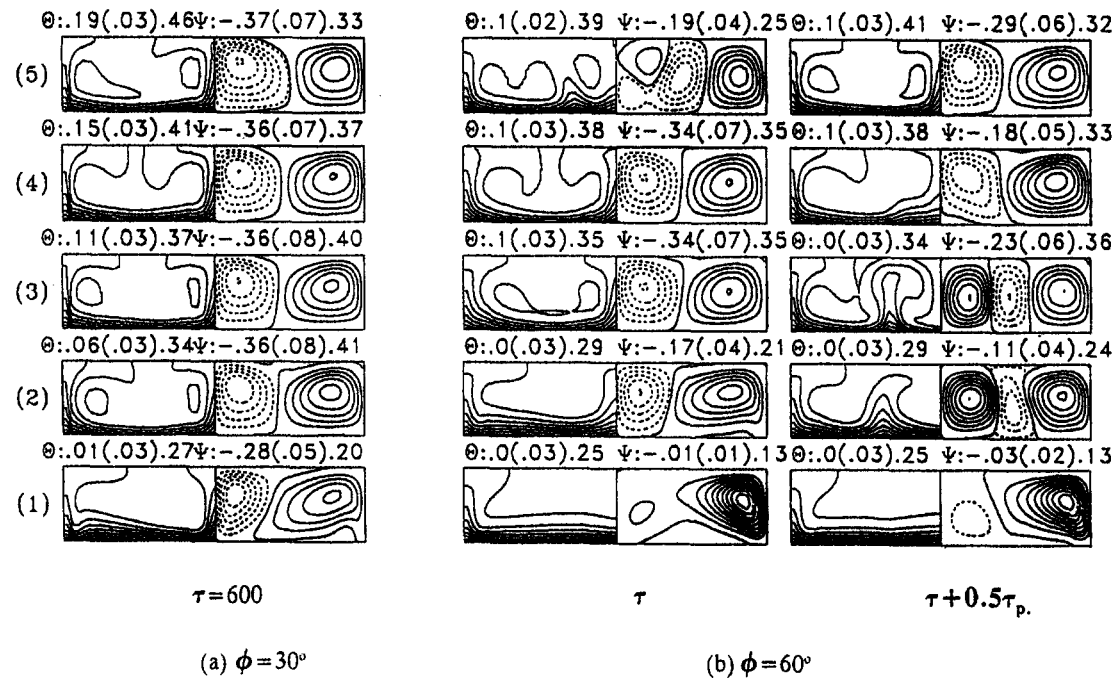

Fig. 8. Isotherms and cross plane streamlines at cross sections (1)$Z = 3.9$, (2)$Z = 6.24$, (3)$Z = 8.58$, (4)$Z = 10.92$ and (5)$Z = 13.26$ at (a) $\tau = 600$ for $\phi = 30°$ and (b) in a typical period ($\tau_p = 16.81$) for $\phi = 60°$, $Re = 100$, $Gr/Re^2 = 90$ and $A = 4$.

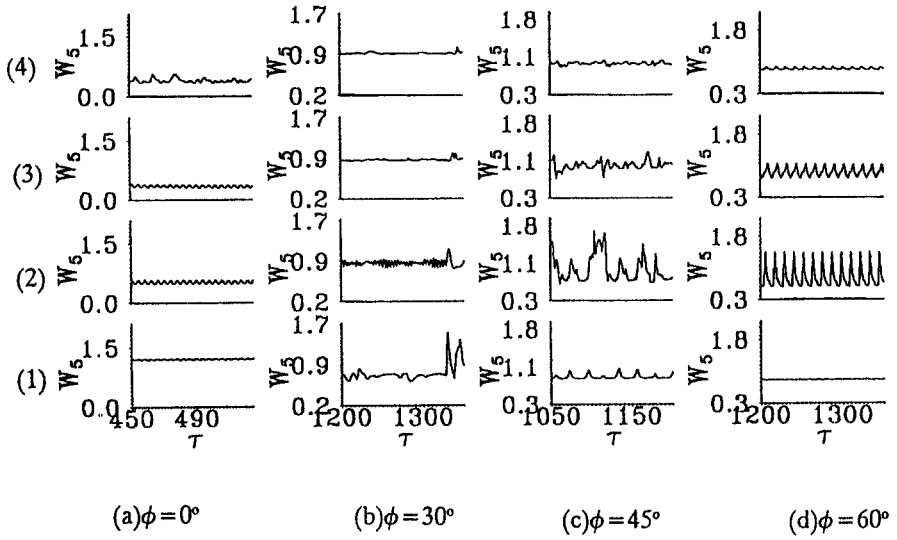

Fig. 9. Time histories of W at location 5 at cross-sections (1)$Z = 3.41$, (2)$Z = 7.32$, (3)$Z = 11.22$ and (4)$Z = 15.12$ for $\phi = 0$, 30, 45 and 60° for $Re = 200$, $Gr/Re^2 = 62.5$ and $A = 4$.

in this region oscillates in a larger amplitude (Fig. 9). Also note that for $\phi = 60°$ the variation of the secondary vortex flow intensity with the axial distance is larger than that for $\phi = 45°$.

To further illustrate the effects of the Reynolds number on the flow transition in an inclined duct, results for a higher Reynolds number are examined in the following. The time histories of θ and W for $Re = 400$, $Gr/Re^2 = 15.625$ and $A = 4$ suggest that at $\phi = 0°$ the flow is time periodic in the entire channel with the decaying oscillation amplitude in the axial direction except in the duct entry ($Z \leqslant 3$). The flow is quasi-periodic in the downstream half of duct at large τ for $\phi = 30°$. At $\phi = 45$ and 60°, a steady flow prevails after the initial transient. The corresponding instantaneous cross plane secondary flow patterns and isotherms at large τ in selected cross sections for $\phi = 0$, 30, 45 and 60° are shown in Fig. 11. Note that for $\phi = 0°$ in the duct entry, four pairs of longitudinal rolls merge into two and in the downstream the flow structure and secondary flow intensity vary only slightly with the downstream distance. As a result, the flow oscillates in a larger amplitude in the duct entry and then decays with the axial distance, as just mentioned. Note that near the duct exit the flow is nearly at steady state.

As the duct is inclined by 30° the flow becomes highly irregular, except in the duct entry. The cells are

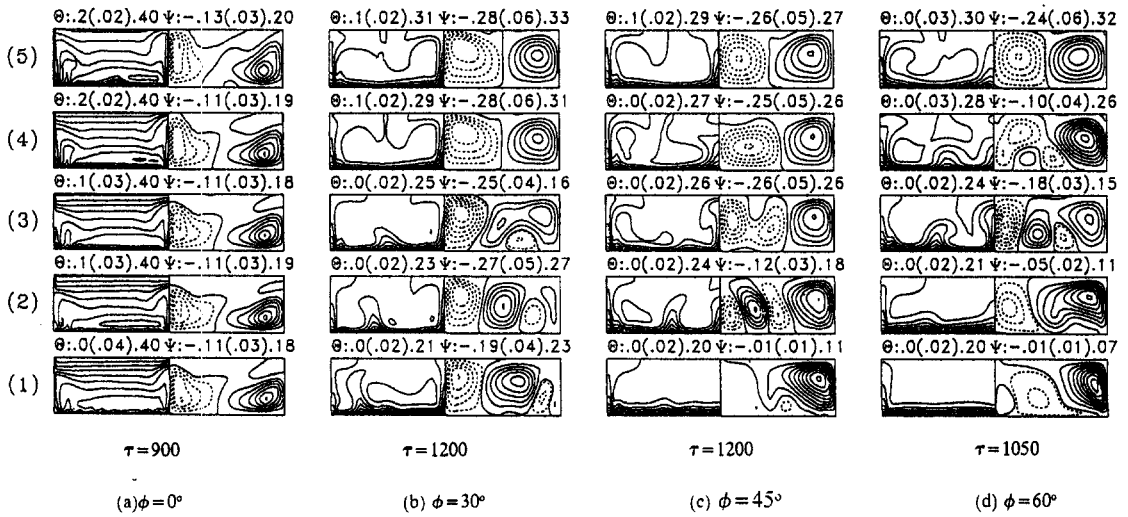

Fig. 10. Isotherms and cross plane streamlines at cross sections (1)$Z = 2.93$, (2)$Z = 4.88$, (3)$Z = 6.83$, (4)$Z = 8.78$ and (5)$Z = 10.73$ for (a) $\phi = 0°$, $\tau = 900$, (b) $\phi = 30°$, $\tau = 1200$, (c) $\phi = 45°$, $\tau = 1200$, (d) $\phi = 60°$, $\tau = 1050$ for $Re = 200$, $Gr/Re^2 = 62.5$ and $A = 4$.

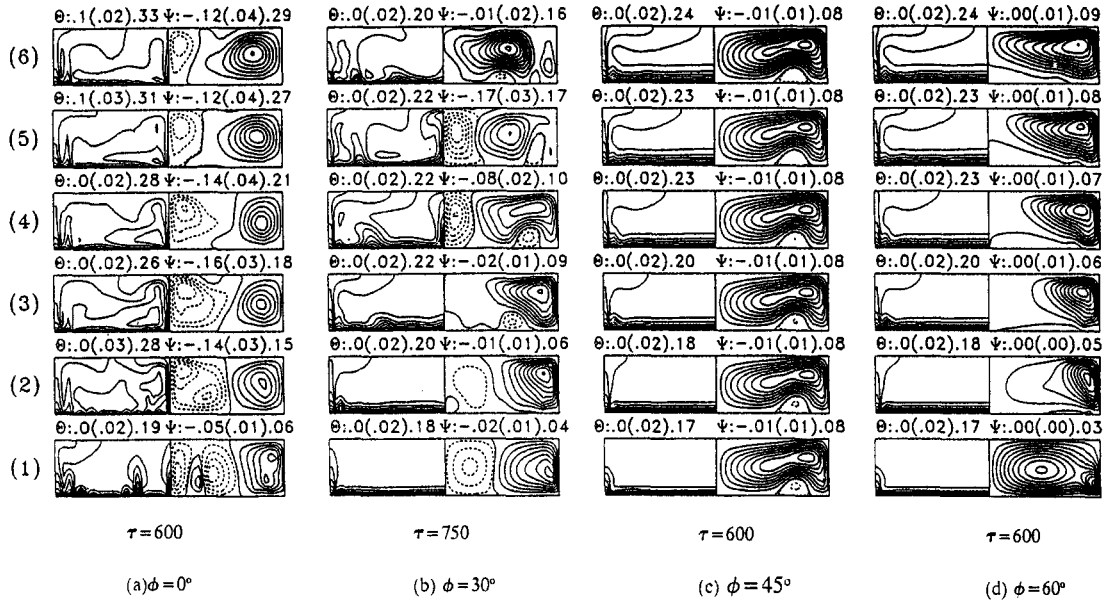

Fig. 11. Isotherms and cross plane streamlines at cross sections (1) $Z = 0.98$, (2) $Z = 2.93$, (3) $Z = 4.88$, (4) $Z = 6.83$, (5) $Z = 8.78$ and (6) $Z = 10.73$ for (a) $\phi = 0°$, $\tau = 600$, (b) $\phi = 30°$, $\tau = 750$, (c) $\phi = 45°$, $\tau = 600$, (d) $\phi = 60°$, $\tau = 600$ for $Re = 400$, $Gr/Re^2 = 15.625$ and $A = 4$.

Table 1. The overall flow characteristics at large τ

A	Pr	Re	Gr/Re^2	ϕ	Flow region		Z^+_{onset} ($\times 10^3$)	Z^+_{hf} ($\times 10^3$)	f_1, f_2 ($1/\tau$)	Pair[a]
2	0.72	500	30	0	$0 \leqslant Z \leqslant 2.4$	SS[b]	5.56	6.7	$f_1 = 0.266$	2
					$2.4 \leqslant Z \leqslant 7.1$	P[c]			$f_2 = 0.320$	
					$7.1 \leqslant Z \leqslant 20$	C[d]				
				30	$0 \leqslant Z \leqslant 2.5$	SS	9.72	6.94	$f_1 = 0.088$	$2 \sim 3$
					$2.5 \leqslant Z \leqslant 20$	P				
				45	$0 \leqslant Z \leqslant 2.93$	SS	12.2	8.13	—	$2 \sim 3$
					$2.93 \leqslant Z \leqslant 20$	C				
				60	$0 \leqslant Z \leqslant 11.2$	SS	23	31.17	$f_1 = 0.092$	2
					$11.2 \leqslant Z \leqslant 20$	P				
4	0.72	100	90	0	$0 \leqslant Z \leqslant 3$	SS	45.8	41.67	$f_1 = 0.077$	$2 \sim 4$
					$3 \leqslant Z \leqslant 20$	P				
				30	$0 \leqslant Z \leqslant 20$	SS	—	—	—	2
				60	$0 \leqslant Z \leqslant 3.41$	SS	—	47.36	$f_1 = 0.059$	$2 \sim 3$
					$3.4 \leqslant Z \leqslant 20$	P				
4	0.72	200	62.5	0	$0 \leqslant Z \leqslant 10.97$	SS	13.2	17.4	$f_1 = 0.267$	$2 \sim 4$
					$10.97 \leqslant Z \leqslant 14.84$	P				
					$14.84 \leqslant Z \leqslant 20$	QP[e]+C				
				45	$0 \leqslant Z \leqslant 2.93$	SS	30.6	—	—	$2 \sim 4$
					$2.93 \leqslant Z \leqslant 20$	QP+C				
				60	$0 \leqslant Z \leqslant 2.93$	SS	37.5	20	$f_1 = 0.087$	$2 \sim 3$
					$2.93 \leqslant Z \leqslant 20$	P				
4	0.72	400	15.625	30	$0 \leqslant Z \leqslant 3.41$	SS	14.9	11.8	—	$2 \sim 3$
					$3.41 \leqslant Z \leqslant 15.12$	P				
					$15.12 \leqslant Z \leqslant 20$	QP+C				
				45	$0 \leqslant Z \leqslant 20$	SS	—	—	—	2
				60	$0 \leqslant Z \leqslant 20$	SS	—	—	—	2

[a] Number of vortex pair(s).
[b] Steady state.
[c] Periodical state.
[d] Chaotic state.
[e] Quasi-periodical state.

rather unstable and their structures change irregularly with time and space. The power spectrum densities for the time records of θ and W indicate that small amplitude periodic flow oscillation prevails in the duct entry. Its frequency is lower than that for $\phi = 0°$. Slightly downstream, the flow oscillates in a large amplitude with the flow being periodic in the duct core region near the central vertical plane at $X = A/2$. But elsewhere it is nonperiodic. Near the duct exit the flow is entirely nonperiodic.

The steady flow pattern shown in Fig. 11 for $\phi = 45°$ indicates that only one pair of longitudinal rolls is induced in the duct. The associated time records of θ and W at various detection points manifest that the initial transient is very short. At an even higher inclined angle of 60°, the resulting flow is also at steady state. The flow pattern is similar to that for $\phi = 45°$.

5. CONCLUDING REMARKS

The above results clearly suggest that the duct inclination has very complex effects on the buoyancy induced flow transition in mixed convective air flows. The flow transition at various inclined angles depends largely on the Reynolds number and aspect ratio of the duct. Sometimes the flow is stabilized by increasing the aiding buoyancy. Other times the reverse is the case. The symmetry breaking processes are not significant in the flow, even if it is in a chaotic state. To provide an overall picture for the flow transition in an inclined duct, the major flow characteristics discussed above are summarized in Table 1.

Acknowledgements—The financial support of this study by the engineering division of Nation Science Council of Taiwan, R.O.C. through the contract NSC83-0404-E009-054 is greatly appreciated. The support of the present computation by the National Center for High-performance Computing and by the computer center of the National Chiao Tung University, Taiwan, Republic of China is also acknowledged.

REFERENCES

1. C. C. Huang and T. F. Lin, Buoyancy induced flow transition in mixed convective flow of air through a bottom heated horizontal duct, *Int. J. Heat Mass Transfer* **37,** 1235–1255 (1994).
2. S. Ostrach and Y. Kamotani, Heat transfer augmentation in laminar fully developed channel flow by means of heating from below, *J. Heat Transfer* **97,** 220–225 (1975).
3. G. J. Hwang and C. L. Liu, An experimental study of convective instability in the thermal entrance region of a horizontal parallel-plate channel heated from below, *Can. J. Chem. Engng* **54,** 521–525 (1976).
4. K. C. Cheng and G. J. Hwang, Numerical solution for combined free and forced laminar convection in horizontal rectangular channels, *J. Heat Transfer* **91,** 59–66 (1969).
5. F. S. Lee and G. J. Hwang, Transient analysis on the onset of thermal instability in the thermal entrance region of a horizontal parallel plate channel, *J. Heat Transfer* **113,** 363–370 (1991).
6. K. C. Chiu and F. Rosenberger, Mixed convection between horizontal plates—I. Entrance effects, *Int. J. Heat Mass Transfer* **30,** 1645–1654 (1987).
7. K. C. Chiu, J. Ouazzani and F. Rosenberger, Mixed convection between horizontal plates—II. Fully developed flow, *Int. J. Heat Transfer* **30,** 1655–1662 (1987).
8. D. G. Osborne and F. P. Incropera, Laminar, mixed convection heat transfer for flow between horizontal parallel plates with asymmetric heating, *Int. J. Heat Mass Transfer* **28,** 207–217 (1985).
9. J. R. Maughan and F. P. Incropera, Experiments on mixed convection heat transfer for airflow in a horizontal and inclined channel, *Int. J. Heat Transfer* **30,** 1307–1318 (1987).
10. F. C. Chou and G. J. Hwang, Vorticity–velocity method for the Graetz problem and the effect of natural convection in a horizontal rectangular channel with uniform wall heat flux, *J. Heat Transfer* **109,** 704–710 (1987).
11. F. P. Incropera and J. A. Schutt, Numerical simulation of laminar mixed convection in the entrance region of horizontal rectangular ducts, *Numer. Heat Transfer* **8,** 707–729 (1985).
12. H. V. Mahaney, F. P. Incropera and S. Ramadhyani, Development of laminar mixed convection flow in a horizontal rectangular duct with uniform bottom heating, *Numer. Heat Transfer* **12,** 137–155 (1987).
13. W. Aung and G. Worku, Mixed convection in ducts with asymmetric wall heat flux, *J.Heat Transfer* **109,** 947–951 (1987).
14. L. C. Chow, S. R. Husain and A. Campo, Effects of free convection and axial conduction on forced convection heat transfer inside a vertical channel at low Peclet numbers, *J. Heat Transfer* **106,** 297–303 (1984).
15. L. S. Yao, Free and forced convection in the entry region of a heated vertical channel, *Int. J. Heat Mass Transfer* **26,** 65–72 (1983).
16. B. R. Morton, D. B. Ingham, D. J. Keen and P. J. Heggs, Recirculating combined convection in laminar pipe flow, *J. Heat Transfer* **111,** 106–113 (1989).
17. D. B. Ingham, D. J. Heggs and B. R. Morton, Recirculating pipe flows, *J. Fluid Mech.* **213,** 443–464 (1990).
18. W. Aung and G. Worku, Theory of fully developed combined convection including flow reversal, *J. Heat Transfer* **108,** 485–488 (1986).
19. D. B. Ingham, D. J. Keen and P. J. Hegges, Two-dimensional combined convection in vertical parallel plate ducts, including situations of flow reversal, *Int. J. Numer. Meth. Engng* **26,** 1645–1664 (1988).
20. K. Fukui, M. Nakajima and H. Ueda, The longitudinal vortex and its effects on the transport processes in combined free and force laminar convection between horizontal and inclined parallel plates, *Int. J. Heat Mass Transfer* **26,** 109–120 (1983).
21. E. Naito and Y. Nagano, The effect of buoyancy on downward and upward laminar-flow convection in the entrance region between inclined parallel plates, *Int. J. Heat Mass Transfer* **32,** 811–823 (1989).
22. S. M. Morcos, M. M. Hilal, M. M. Kamel and M. S. Soliman, Experimental investigation of mixed laminar convection in the entrance region of inclined rectangular channels, *Int. J. Heat Mass Transfer* **108,** 574–579 (1986).
23. J. Argyris, G. Faust and M. Haase, An adventure in chaos, *Comput. Meth. Appl. Mech. Engng* **91,** 997–1091 (1991).
24. D. B. Holes and J. R. Vermmeulen, Velocity profiles in ducts with rectangular cross sections, *Chem. Engng Sci.* **23,** 717–722 (1968).
25. R. Peyret and T. D. Taylor, *Computational Methods For Fluid Flow*, Chap. 6. Springer, New York (1983).

26. D. C. Hirsch, Numerical computation of internal and external flow, Vol. 1, pp. 176–179. Wiley, New York (1989).
27. T. Kawamura, H. Takami and K. Kuwahara, New higher-order upwind scheme for incompressible Navier–Stokes equations, *9th ICNMFD* **10,** 285–291 (1985).
28. D. A. Anderson, J. C. Tannehill and R. H. Pletcher, *Computational Fluid Mechanics and Heat Transfer*, pp. 71–77. Hemisphere, Washington DC (1984).
29. T. F. Lin, Thermal control of microelectronic equipment D buoyancy driven unsteady mixed convection in rectangular channel (II) NSC 81-0404-009-101, Hsinchu, Taiwan, Republic of China (1982).